Graphical Abstract

A hyperelastic beam model for the photo-induced response of nematic liquid crystal elastomers

Farzam Dadgar-Rad,Mohammad Mehdi Mahjoub,Mokarram Hossain

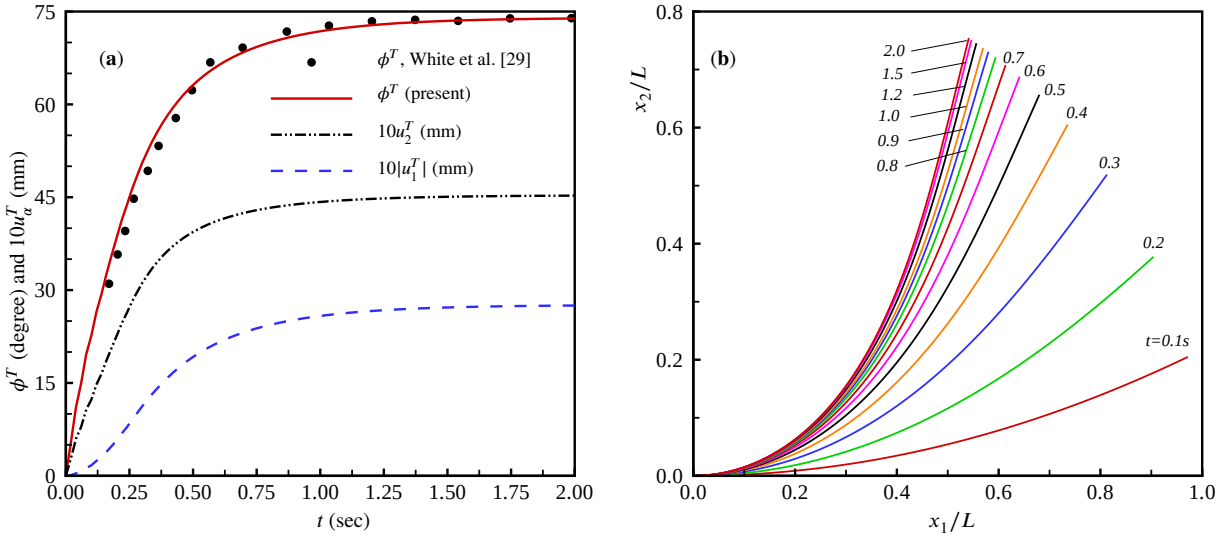

Figure 2. (**a**): Time history of the slope angle ϕ and the displacement components $|u_1|$ and u_2 at the tip point T of the LCE beam, (**b**): deformed shapes of the beam for $t \in \{0.1, 0.2, ..., 0.9, 1, 1.2, 1.5, 2\}$ (s)

In this example, we consider a cantilever beam composed of LCEs subjected to light loading above its top surface. This scenario has been experimentally investigated by White et al. [29]. The apparent intensity of the light is $\mathcal{I}_0 = 1000$ mW/cm^2. The length, width, and height of the beam are $L = 6$ mm, $b = 1$ mm, and $h = 8$ μm, respectively. Variation of the tip slope angle ϕ^T, and the tip displacement components $|u_1^T|$ and u_2^T (scaled by 10) of the beam are displayed in the left panel. The maximum values of the mentioned parameters are obtained to be $\phi^T_{\max} = 73.87°$, $u^T_{1\max} = 2.75$ mm, and $u^T_{2\max} = 4.53$ mm, respectively. Moreover, it is observed that the curve corresponding to the time history of the tip slope angle ϕ^T are in good agreement with the experimental data reported in the literature. Furthermore, deformed shapes of the beam at various time values, namely $t \in \{0.1, 0.2, ..., 0.9, 1, 1.2, 1.5, 2\}$ (s) are illustrated in the right panel.

Highlights

A hyperelastic beam model for the photo-induced response of nematic liquid crystal elastomers

Farzam Dadgar-Rad,Mohammad Mehdi Mahjoub,Mokarram Hossain

- A hyperelastic beam model for analyzing large deformations in thin and slender LCEs under illumination has been developed.
- The formulation is applicable to ideal, non-ideal, isotropic genesis, and nematic genesis LCEs.
- A total Lagrangian FE formulation for the numerical solution of the problems is developed.
- The numerical results align excellently with the data available in the literature.

A hyperelastic beam model for the photo-induced response of nematic liquid crystal elastomers

Farzam Dadgar-Rad[a,*], Mohammad Mehdi Mahjoub[a] and Mokarram Hossain[b]

[a]Faculty of Mechanical Engineering, University of Guilan, Rasht, 695013, Guilan, Iran
[b]Zienkiewicz Institute for Modelling, Data and AI, Faculty of Science and Engineering, Swansea University, SA1 8EN, UK

ARTICLE INFO

Keywords:
Liquid crystalline elastomer
Nematic mesogens
Beams
Photo-actuation
Finite element method

ABSTRACT

Liquid crystal elastomers (LCEs) are a novel class of materials created by combining polymeric solids with stiff, rod-like molecules known as nematic mesogens. These materials exhibit large, reversible deformations under mechanical, thermal, and optical stimuli. In this work, we develop a nonlinear beam formulation for analyzing the finite elastic deformation of beam-like structures made of LCEs under photo-actuation. This formulation applies to ideal, non-ideal, isotropic genesis, and nematic genesis LCEs. We establish the variational form of the problem based on the principle of virtual work. To solve numerical examples, we also develop a nonlinear finite element formulation based on B-spline functions. Several numerical examples are presented to demonstrate the applicability of the proposed formulation.

1. Introduction

Liquid crystal elastomers (LCEs) are a novel class of polymeric materials that merge the elastic deformability of elastomers with the orientational properties of liquid crystals [1, 2]. Elastomers are filled with liquid crystalline mesogens, which are rod-like and stiff molecules. If the mesogens are dispersed almost isotropically within the elastomeric medium in the undeformed state, the LCE is termed isotropic genesis. Otherwise, it is termed nematic genesis. These materials have been applied across various advanced technologies due to their capacity to undergo substantial shape transformations in response to light and other stimuli. For example, LCEs are utilized in soft robotic systems to develop actuators that replicate muscle movements. Their light-responsive properties allow for precise motion control, enabling the creation of robots capable of moving, gripping, or manipulating objects with high accuracy (e.g., Refs. [3, 4]). Additionally, LCEs are used in the fabrication of tunable optical components, such as lenses, diffraction gratings, adaptive optics, and dynamic display technologies [4, 5]. Moreover, due to their biocompatibility and ability to simulate biological tissues, LCEs are being investigated for applications in medical implants and devices, including stents and spinal fusion cages [6, 7]. Furthermore, the photoresponsive behavior of LCEs enables the development of materials that alter their properties or appearance under specific lighting conditions, making them ideal for information encryption [8, 9]. Notable research on the synthesis and experimental analysis of LCEs has been conducted by Finkelmann and his coworkers (e.g., Refs. [10–15]). LCEs exhibit reversible finite

*Corresponding author
dadgar@guilan.ac.ir (F. Dadgar-Rad); mahjoub.mohammadmehdi@gmail.com (M.M. Mahjoub); mokarram.hossain@swansea.ac.uk (M. Hossain)
ORCID(s): 0000-0003-1546-2446 (F. Dadgar-Rad); 0009-0007-3662-0825 (M.M. Mahjoub); 0000-0002-4616-1104 (M. Hossain)

deformations in response to mechanical [16–24], thermal [25–27], and optical [28–35] stimuli. Developing efficient theoretical and numerical formulations to predict the behavior of structures made from LCEs is crucial for the optimal and effective design of sensors, actuators and other devices. Accordingly, in this work, a nonlinear model along with its finite element formulation is developed for the large elastic deformation analysis of beam-like structures made of LCEs and actuated by light. Several general continuum-based formulations for the analysis of LCEs have been developed in the literature (e.g., [2, 36–42]). Notably, the formulation proposed by Zhang et al. [2] includes viscoelastic effects. Anderson et al. [36] introduced orientational momentum balance equations in addition to classical deformational momentum balance equations. Fried and Sellers [40] proposed several forms of the free energy density function, with and without contributions from volume change. The formulation by Brighenti et al. [41] is a micromechanical-based model focusing on the evolution of the chain distribution tensor of the LCE network. DeSimone and his colleagues [43–45] pointed out that the neo-classical free energy density introduced by Bladon et al. [46] is not convex, leading them to introduce the concept of quasi-convexification of the free energy density of LCEs.

Extensive research has been conducted on the deformation of structures made of LCEs. The deformation of LCE membranes has been examined in Refs. [47–54]. Additionally, LCE plates have been analyzed in Refs. [55–59]. Several LCE beam formulations, particularly those emphasizing light-induced deformation, have also been proposed (e.g., Refs. [52, 60–69]). Specifically, the models developed in Refs. [62–65] focus on the infinitesimal deformation of LCE beams. Moderately large deformations considering the von-Karman strain tensor have been investigated in Ref. [66]. Assuming the nematic field in an undeformed state is isotropic, Goriely et al. [68] developed a 3D beam model based on the decomposition of the deformation gradient into an elastic part and a liquid crystalline part called the confirmation or step-length tensor. The model proposed by Norouzikudiani et al. [69] incorporates both thermal and light effects.

A survey of the literature reveals that most formulations for LCE beams are simplistic and restricted to infinitesimal deformations, while these structures exhibit finite deformations under photo-actuation in most cases. Many formulations do not begin with the strain energy density function of LCEs, relying instead on the relation $M = EI(\kappa - \kappa_0)$ between the bending moment M, total curvature κ, photo-induced curvature κ_0, and bending rigidity EI. Furthermore, the incompressibility of LCEs is often neglected in these formulations. Additionally, a comprehensive and reliable computational formulation for the numerical solution of this problem has not yet been proposed in the literature. Accordingly, the main novelties of this work are as follows:

- The formulation is based on the hyperelastic nature of LCEs, with the strain energy density of these materials playing a crucial role in both the variational and numerical formulations.
- The incompressibility constraint is exactly satisfied in the present formulation.

- The effect of finite photo-induced strain is included in the current step-length tensor, which leads to the classical results at infinitesimal deformations.
- The formulation is applicable to all types of LCEs, including ideal, non-ideal, isotropic genesis, and nematic genesis types.

The remaining sections of this work are organized as follows: Section 2 presents the basic kinematic quantities of the beam model, taking light effects into account. In Section 3, the free energy density function and the variational formulation of LCE beams are developed. Section 4 introduces a total Lagrangian nonlinear finite element formulation based on B-splines. Numerical examples are solved in Section 5 to evaluate the applicability of the proposed formulation. Finally, a summary of the work is provided in Section 6.

Notation: In this work, Greek and Latin indices obey Einstein's summation convention and take $\{1,2\}$ and $\{1,2,3\}$, respectively. Upper-case calligraphic indices, e.g., $\mathcal{J}$, do not follow a general rule and take the values exactly specified in the corresponding equations. For two second-order tensors $\mathbf{A}$ and $\mathbf{B}$, the tensorial products of the form $(\mathbf{A}\otimes\mathbf{B})_{ijkl} = A_{ij}B_{kl}$, $(\mathbf{A}\boxtimes\mathbf{B})_{ijkl} = A_{ik}B_{lj}$, and $(\mathbf{A}\odot\mathbf{B})_{ijkl} = A_{il}B_{kj}$ are defined. Moreover, the notation $\boldsymbol{\mathcal{A}}_{,\boldsymbol{\mathcal{B}}}$ denotes the partial derivative of the tensor quantity $\boldsymbol{\mathcal{A}}$ with respect to the tensor $\boldsymbol{\mathcal{B}}$, namely $\boldsymbol{\mathcal{A}}_{,\boldsymbol{\mathcal{B}}} = \partial\boldsymbol{\mathcal{A}}/\partial\boldsymbol{\mathcal{B}}$.

2. Kinematics of the LCE beam model

Let the point sets $\mathcal{B}_0$ and $\mathcal{B}_t$ represent the reference and current configurations of a beam made of LCEs at times $t = 0$ and $t > 0$, respectively. To describe the beam deformation, as shown in Fig. 1, two common-frame rectangular Cartesian coordinate systems X_1, X_2, X_3 and x_1, x_2, x_3 are positioned at the centroid of the left end of the beam. The beam lies in the X_1X_2 plane, so that the coordinate lines X_1, X_2, and X_3 are directed along the beam's centerline, thickness, and width, respectively. The basis vectors of both coordinate systems are denoted by the triad $\mathbb{e}_1, \mathbb{e}_2, \mathbb{e}_3$.

The vector $\mathbb{X} = X_1\mathbb{e}_1 + X_2\mathbb{G}$, with $\mathbb{G} = \mathbb{e}_2$ as the reference director, characterizes the position vector of an undeformed material particle in the X_1X_2 plane. The material points on the undeformed centerline are described by the vector $\mathbb{X} = X_1\mathbb{e}_1$. It is well known that in the Timoshenko beam model, a plane cross-section remains plane during deformation. In this work, the following Timoshenko-type deformation field is considered (see, e.g., Refs. [70, 71]):

$$\mathbb{x} = \bar{\mathbb{x}}(X_1,t) + \big[X_2 + X_2^2\eta(X_1,t)\big]\mathbb{g}(X_1,t). \tag{1}$$

Here, $\bar{\mathbb{x}}$ is the position vector on the deformed centerline, $\mathbb{g}$ is the deformed director that signifies the cross-section rotation, and the scalar function η describes the through-thickness stretching of the beam. Motivated by the expressions for the reference and current position vectors $\mathbb{X}$ and $\mathbb{x}$, the displacement vector of the centerline, $\mathbb{u}$, and the director

difference vector, $\mathbb{w}$, are defined as follows:

$$\mathbb{u} = u_\alpha \mathbb{e}_\alpha = \bar{\mathbb{x}} - \mathbb{X}, \qquad \mathbb{w} = w_\alpha \mathbb{e}_\alpha = \mathbb{g} - \mathbb{G}, \tag{2}$$

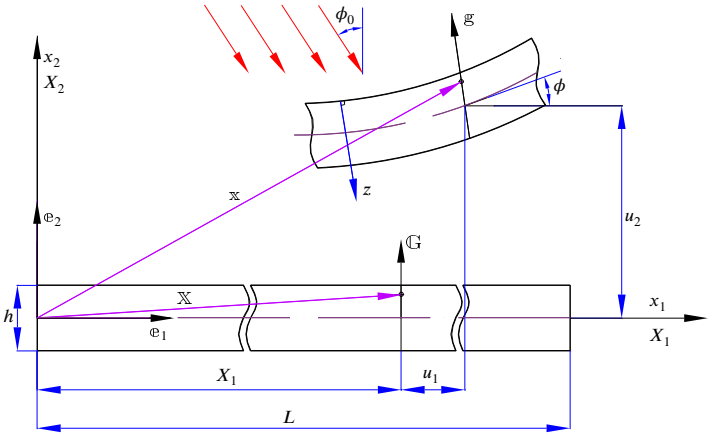

Figure 1: Deformation of an LCE beam under illumination

Based on Eq. (1), the deformation gradient tensor $\mathbf{F} = \mathrm{Grad}\,\mathbb{x}$ is calculated as follows:

$$\mathbf{F} = \begin{bmatrix} F_{11} & F_{12} & 0 \\ F_{21} & F_{22} & 0 \\ 0 & 0 & \lambda \end{bmatrix}, \tag{3}$$

where λ is the stretch in the X_3 direction, and the planar components $F_{\alpha\beta}$ of $\mathbf{F}$ are given by

$$F_{11} = 1 + u_1' + X_2 w_1', \quad F_{12} = (1 + 2X_2\eta)w_1, \quad F_{21} = u_2' + X_2 w_2', \quad F_{22} = (1 + 2X_2\eta)(1 + w_2). \tag{4}$$

It should be noted that the higher-order terms involving X_2^2 are neglected. Additionally, a superimposed prime denotes differentiation with respect to X_1. LCEs, like other polymeric materials, are generally assumed to be incompressible, namely $J = \det \mathbf{F} = 1$ [1, 72]. From this assumption, the thickness stretch λ can be written as

$$\lambda = \hat{J}^{-1} \quad \text{with} \quad \hat{J} = F_{11}F_{22} - F_{12}F_{21}. \tag{5}$$

In the next step, let $\mathbb{n}_0$ and $\mathbb{n}$ be the unit vectors that determine the direction of nematic mesogens in the reference and current configurations, respectively. In the present beam formulation, it is assumed that $\mathbb{n}_0$ and $\mathbb{n}$ are always parallel with the X_1X_2-plane. Therefore, as shown in Fig. 1, they can be expressed in terms of the angles $\theta_0(X_1)$ and $\theta(X_1)$ as

follows:

$$\mathbb{m}_0 = c_0\mathbb{e}_1 + s_0\mathbb{e}_2, \quad \mathbb{m} = c\mathbb{e}_1 + s\mathbb{e}_2 \quad \text{with} \quad c_0 = \cos\theta_0, \quad s_0 = \sin\theta_0, \quad c = \cos\theta, \quad s = \sin\theta. \tag{6}$$

Besides the deformation gradient tensor $\mathbf{F}$, the deformation of LCEs is highly dependent upon the step length tensors $\mathbf{L}_0$ and $\mathbf{L}$, respectively, in the reference and current configurations. In this work, the expressions for $\mathbf{L}_0$ and $\mathbf{L}$ are written in the following form (see, e.g., [1, 38, 53]):

$$\mathbf{L}_0 = R_0^{-1}\mathbf{I} + \left(R_0^2 - R_0^{-1}\right)\mathbf{N}_0, \quad \mathbf{L} = R^{-1}\mathbf{I} + \left(R^2 - R^{-1}\right)\mathbf{N}, \tag{7}$$

where $\mathbf{I}$ is the identity tensor in the 3D space. Moreover, the quantities denoted by $\mathbf{N}_0$, $\mathbf{N}$, R_0, and R are defined as follows:

$$\mathbf{N}_0 = \mathbb{m}_0 \otimes \mathbb{m}_0, \quad \mathbf{N} = \mathbb{m} \otimes \mathbb{m}, \quad R_0 = r_0^{1/3}, \quad R = r^{1/3}. \tag{8}$$

Here r_0 and r represent the referential and current anisotropy parameters, respectively. In the special case where $r_0 = 1$, one obtains $\mathbf{L}_0 = \mathbf{I}$, signifying that the LCE is in isotropic state in the reference configuration. In contrast, from $r^* = 1$ it follows that $\mathbf{L} = \mathbf{I}$ and the LCE is in isotropic state in the current configuration. It can be easily verified that the inverse of the current length step tensor $\mathbf{L}$, denoted here by $\tilde{\mathbf{L}}(\theta, R)$, is given by

$$\tilde{\mathbf{L}} \overset{\text{def}}{=} \mathbf{L}^{-1} = R\mathbf{I} + k\mathbf{N} \quad \text{with} \quad k = R^{-2} - R. \tag{9}$$

For optical loading, it is assumed that the light intensity $\mathcal{I}$ decreases exponentially through the thickness of the LCE beam. As illustrated in Fig. 1, let $z = h/2 - X_2$ represent the coordinate along the beam's thickness. Under this assumption, the intensity $\mathcal{I}$ will be proportional to $\exp(-\hat{k}z)$, where $\hat{k}$ is a constant. Specifically, assuming that the light intensity is $\mathcal{I}_0$ at the top surface (i.e., at $z = 0$), the expression for $\mathcal{I}$ through the beam thickness is approximately given by (e.g., Refs. [66, 67, 73, 74]):

$$\mathcal{I}(z) = \mathcal{I}_0 \exp\left(-\frac{z}{d}\right) = \mathcal{I}_0 \exp\left(\frac{X_2 - h/2}{d}\right), \tag{10}$$

where $\mathcal{I}_0$ is the light intensity at the top surface of the beam (i.e., at $X_2 = h/2$), and $d = 1/\hat{k}$ is the light penetration depth. It is noted that at $z = d$, the light intensity will be $\mathcal{I}|_{z=d} = \mathcal{I}_0 \exp(-1) \approx 0.37\mathcal{I}_0$.

Under illumination, the initially straight dye molecules, referred to as *trans*, bend into *cis* ones. If $n_{\mathfrak{t}}$ and $n_{\mathfrak{c}}$ denote, respectively, the *trans* and *cis* fractions of the dye molecules, then the relation $n_{\mathfrak{t}} + n_{\mathfrak{c}} = 1$ holds. The differential

equation governing the *cis* fraction $n_{\mathfrak{c}}$ can be expressed as follows (see also Ref. [67]):

$$\tau \frac{\partial n_{\mathfrak{c}}(t)}{\partial t} + (1+K) n_{\mathfrak{c}}(t) = K \quad \text{with} \quad K = \frac{\mathcal{I}}{\mathcal{I}_{\mathfrak{c}}} \quad \text{and} \quad \mathcal{I}_{\mathfrak{c}} = \frac{1}{\tau \Gamma}. \tag{11}$$

where τ represents the *cis* state lifetime, Γ stands for the adsorption constant, and $\mathcal{I}_{\mathfrak{c}}$ is referred to as the characteristic light intensity [60, 68]. Using the initial condition $n_{\mathfrak{c}}(0) = 0$, the solution for $n_{\mathfrak{c}}$ is as follows:

$$n_{\mathfrak{c}}(t) = \frac{K}{1+K} \Big\{ 1 - \exp\Big[-(1+K) \frac{t}{\tau} \Big] \Big\}. \tag{12}$$

It is worth noting that in most cases, K is a small quantity, allowing for the approximate relation $1 + K \approx 1$ to be employed in various studies (e.g., Ref. [66]). However, in this work, such an approximation has not been utilized. Adopting the approach outlined by Korner et al. [67], the intensity $\mathcal{I}_0$ is adjusted to incorporate the effect of the relative orientation between light and the beam surface, resulting in $\mathcal{I}_0 f(\phi - \phi_0)$. Here, ϕ denotes the slope angle of the beam, while ϕ_0 represents the illumination angle, as depicted in Fig. 1. It is noted that the thickness of LCE beams typically ranges from 5 to 20 microns, which is extremely thin compared to conventional engineering beams. Additionally, LCE beams are highly slender, with aspect ratios (length-to-height ratios) often exceeding 500, as illustrated in the examples in Subsections 5.1 and 5.3, based on experiments from Refs. [29, 30]. Consequently, due to their minimal thickness and large aspect ratio, the slope on the top surface of an LCE beam can be approximated by the slope at its centerline. The slope angle ϕ and the function f are given as follows:

$$\phi(u_1, u_2) = \operatorname{atan}\left(\frac{\mathrm{d}x_2}{\mathrm{d}x_1} \right) = \operatorname{atan}\left(\frac{\partial x_2 / \partial X_1}{\partial x_1 / \partial X_1} \right) = \operatorname{atan}\left(\frac{u_2'}{1 + u_1'} \right), \tag{13}$$

$$f(\bar{\phi}) = \langle \bar{\phi} \rangle \cos \bar{\phi} \quad \text{with} \quad \langle \bar{\phi} \rangle \overset{\text{def}}{=} \begin{cases} 1 & \text{for} \quad \bar{\phi} \in (-\pi/2, \pi/2), \\ 0 & \text{otherwise.} \end{cases} \tag{14}$$

where $\bar{\phi} = \phi - \phi_0$. The bending-type transformation of dye molecules induces the photo strain $\boldsymbol{\varepsilon}_{\parallel}^{\mathfrak{ph}}$ along the director $\mathbb{m}$, given by

$$\boldsymbol{\varepsilon}_{\parallel}^{\mathfrak{ph}} = -C_{\mathfrak{ch}} n_{\mathfrak{c}} = -\frac{K^* \langle \bar{\phi} \rangle \cos \bar{\phi}}{1 + K \langle \bar{\phi} \rangle \cos \bar{\phi}} \quad \text{with} \quad K^* = C_{\mathfrak{ch}} K \Big\{ 1 - \exp\Big[-(1+K) \frac{t}{\tau} \Big] \Big\}, \tag{15}$$

where $C_{\mathfrak{ch}}$ represents the chemical contraction coefficient.

At the infinitesimal regime of deformations, the small strain tensor $\boldsymbol{\varepsilon}$ is additively decomposed as $\boldsymbol{\varepsilon} = \boldsymbol{\varepsilon}^{\mathfrak{e}} + \boldsymbol{\varepsilon}^{\mathfrak{p}\mathfrak{h}}$ (e.g., [58, 63]). Here, $\boldsymbol{\varepsilon}^{\mathfrak{e}}$ and $\boldsymbol{\varepsilon}^{\mathfrak{p}\mathfrak{h}}$ represent the elastic and photo-induced parts of the strain, respectively. Specifically, the expression for the photo strain tensor $\boldsymbol{\varepsilon}^{\mathfrak{p}\mathfrak{h}}$ is given by

$$\boldsymbol{\varepsilon}^{\mathfrak{p}\mathfrak{h}} = \varepsilon_{\perp}^{\mathfrak{p}\mathfrak{h}}\mathbf{I} + (\varepsilon_{\parallel}^{\mathfrak{p}\mathfrak{h}} - \varepsilon_{\perp}^{\mathfrak{p}\mathfrak{h}})\mathbf{N} \quad \text{with} \quad \varepsilon_{\perp}^{\mathfrak{p}\mathfrak{h}} = -\nu^{\mathfrak{p}\mathfrak{h}}\varepsilon_{\parallel}^{\mathfrak{p}\mathfrak{h}}. \tag{16}$$

Here, $\varepsilon_{\perp}^{\mathfrak{p}\mathfrak{h}}$ is the photo strain component perpendicular to the director $\mathbb{n}$. Moreover, $\nu^{\mathfrak{p}\mathfrak{h}}$ is the light-induced Poisson's ratio and is often considered to be $\frac{1}{2}$. In particular, by assuming that the unit director vector $\mathbb{n}$ is the first basis vector of a Cartesian coordinate system, the expression for the photo strain tensor $\boldsymbol{\varepsilon}^{\mathfrak{p}\mathfrak{h}}$ reduces to

$$\boldsymbol{\varepsilon}^{\mathfrak{p}\mathfrak{h}} = \operatorname{diag}\big[1, -\tfrac{1}{2}, -\tfrac{1}{2}\big]\varepsilon_{\parallel}^{\mathfrak{p}\mathfrak{h}}. \tag{17}$$

Now, it is assumed that the stretch parameter R in the current step length tensor $\mathbf{L}$ is the updated value of R_0 via the following relation:

$$R = R_0 + \varepsilon_{\parallel}^{\mathfrak{p}\mathfrak{h}}. \tag{18}$$

If $R_0 = 1$ and assuming that $\varepsilon_{\parallel}^{\mathfrak{p}\mathfrak{h}}$ is small, it then follows that

$$R^2_{|_{\mathfrak{inf}}} = 1 + 2\varepsilon_{\parallel}^{\mathfrak{p}\mathfrak{h}}, \quad R^{-1}_{|_{\mathfrak{inf}}} = 1 - \varepsilon_{\parallel}^{\mathfrak{p}\mathfrak{h}}, \tag{19}$$

where the subscript $\mathfrak{inf}$ denotes infinitesimal deformations. Now, from Eqs. (7), (9), (15), and (19) the expressions for $\mathbf{L}$ and $\tilde{\mathbf{L}}$ at infinitesimal deformations are obtained as:

$$\mathbf{L}_{|_{\mathfrak{inf}}} = \mathbf{I} + 2\boldsymbol{\varepsilon}^{\mathfrak{p}\mathfrak{h}}, \quad \tilde{\mathbf{L}}_{|_{\mathfrak{inf}}} = \mathbf{I} - 2\boldsymbol{\varepsilon}^{\mathfrak{p}\mathfrak{h}}. \tag{20}$$

3. Free energy density of LCEs and variational formulation

To express the free energy of LCEs, we introduce the second-order tensors $\boldsymbol{\Lambda}$ and $\boldsymbol{\Psi}$ as follows:

$$\boldsymbol{\Lambda} = \tilde{\mathbf{L}}\mathbf{F}\mathbf{L}_0\mathbf{F}^{\mathsf{T}}, \quad \boldsymbol{\Psi} = \mathbf{N}\mathbf{F}\bar{\mathbf{N}}_0\mathbf{F}^{\mathsf{T}}, \tag{21}$$

where the tensor $\bar{\mathbf{N}}_0 = \mathbf{I} - \mathbf{N}_0$ is defined for simplicity in notation. In the literature, the tensor $\boldsymbol{\Lambda}$ is often referred to as the *relative strain* or, more accurately, *relative deformation* tensor (e.g., [37, 38]).

Remark 1: For regular materials with $\mathbf{L} = \mathbf{L}_0 = \mathbf{I}$, the tensor $\boldsymbol{\Lambda}$ reduces to the left Cauchy–Green deformation tensor $\mathbf{B} = \mathbf{F}\mathbf{F}^{\mathsf{T}}$. It is well-known that at infinitesimal deformations, the deformation gradient tensor reduces to $\mathbf{F}_{|_{\mathrm{inf}}} = \mathbf{I}+\boldsymbol{\varepsilon}+\boldsymbol{\Omega}$, where $\boldsymbol{\Omega}$ is the infinitesimal rotation tensor. Accordingly, due to the symmetry of $\boldsymbol{\varepsilon}$ and skew-symmetry of $\boldsymbol{\Omega}$, the tensor $\mathbf{B}$ at small deformations reduces to $\mathbf{B}_{|_{\mathrm{inf}}} = \mathbf{I} + 2\boldsymbol{\varepsilon}$.

Remark 2: If $\mathbf{L}_0 = \mathbf{I}$, at infinitesimal deformations, from Eqs. (20), $(21)_1$, the expression for the relative deformation tensor $\boldsymbol{\Lambda}$ reduces to $\boldsymbol{\Lambda}_{|_{\mathrm{inf}}} = \mathbf{I} + 2(\boldsymbol{\varepsilon} - \boldsymbol{\varepsilon}^{\mathfrak{p}\mathfrak{h}}) = \mathbf{I} + 2\boldsymbol{\varepsilon}^{\mathfrak{e}}$.

In this work, the free energy density function $\mathcal{U}$ of LCEs is expressed as follows:

$$\mathcal{U}(\mathbf{F}, \theta, \phi) = \mathcal{U}^{\mathfrak{e}} - P^*(J - 1) \quad \text{with} \quad \mathcal{U}^{\mathfrak{e}} = \mathcal{U}^{\mathfrak{i}}(\boldsymbol{\Lambda}) + \mathcal{U}^{\mathfrak{ni}}(\boldsymbol{\Psi}). \tag{22}$$

Here, $\mathcal{U}^{\mathfrak{i}}(\boldsymbol{\Lambda})$ represents the ideal (or neo-classical) energy density, and $\mathcal{U}^{\mathfrak{ni}}(\boldsymbol{\Psi})$ accounts for the non-ideal or semi-soft contribution. Moreover, P^* acts as the Lagrange multipliers to enforce the incompressibility condition $J = 1$. It is worth noting that the effect of the slope angle ϕ has been incorporated in the formulation. The expressions for $\mathcal{U}^{\mathfrak{i}}$ and $\mathcal{U}^{\mathfrak{ni}}$ are as follows ([1, 46, 53, 75, 76]):

$$\mathcal{U}^{\mathfrak{i}} = \frac{1}{2}\mu(\mathrm{tr}\,\boldsymbol{\Lambda} - 3), \quad \mathcal{U}^{\mathfrak{ni}} = \frac{1}{2}\alpha\mu(\mathrm{tr}\,\boldsymbol{\Psi} - 3), \tag{23}$$

where μ denotes the shear modulus, and α represents the non-ideality parameter.

It is noted that the neo-classical energy density $\mathcal{U}^{\mathfrak{i}}$ has been derived under the assumption of a Gaussian distribution of chains. However, as pointed out by Biggins et al.[75], real chains are neither perfectly Gaussian nor entirely compositionally homogeneous. Real elastomers, cross-linked in the nematic state, retain a memory of the director $\mathbb{n}_0$ at the time of cross-linking and minimize their free energy when their director aligns with this direction. This effect is captured by incorporating the non-ideal term $\mathcal{U}^{\mathfrak{ni}}$, as proposed by Verwey and Warner[76], into the free energy, which promotes the alignment of the director along $\mathbb{n}_0$.

Remark 3: Let $\boldsymbol{\Upsilon} = \mathrm{Grad}\,\mathbb{n} = \theta'(-s\mathbb{e}_1 \otimes \mathbb{e}_1 + c\mathbb{e}_2 \otimes \mathbb{e}_1)$ be a second-order tensor that describes the gradient of the current director vector. A simplified form of the Frank energy density [77], given by $\mathcal{U}^{\mathfrak{f}}(\boldsymbol{\Upsilon}) = \frac{1}{2}k^{\mathfrak{f}}\theta'^2$, could be added to the free energy density function (e.g., Zhang et al. [2]). Here, $k^{\mathfrak{f}}$ denotes the Frank constant. However, in existing LCEs, the effect of Frank energy is negligible and is not considered in the present study.

From Eqs. (22) and (23), the virtual free energy density can be expressed as

$$\delta\mathcal{U}(\mathbf{F}, \theta, \phi) = \mathbf{P} : \delta\mathbf{F} + Q\delta\theta + T\delta\phi, \tag{24}$$

where the first Piola–Kirchhoff stress $\mathbf{P}$, and the quantities Q and T are as follows:

$$\left.\begin{aligned} \mathbf{P} = \mathcal{U}_{,\mathbf{F}} = \mathcal{U}^{\mathrm{e}}_{,\mathbf{F}} - P^* \left(J_{,\mathbf{F}}\right)_{J=1} = \mu(\tilde{\mathbf{L}}\mathbf{F}\mathbf{L}_0 + \alpha\mathbf{N}\mathbf{F}\bar{\mathbf{N}}_0) - P^*\mathbf{F}^{-\top} \\ Q = \mathcal{U}_{,\theta} = \frac{1}{2}\mu \mathrm{tr}\left(\tilde{\mathbf{L}}_{,\theta}\mathbf{F}\mathbf{L}_0\mathbf{F}^{\top} + \mathbf{N}_{,\theta}\mathbf{F}\bar{\mathbf{N}}_0\mathbf{F}^{\top}\right) \\ T = \mathcal{U}_{,\phi} = \frac{1}{2}\mu \mathrm{tr}\left(\tilde{\mathbf{L}}_{,\phi}\mathbf{F}\mathbf{L}_0\mathbf{F}^{\top}\right) \end{aligned}\right\}. \tag{25}$$

Moreover, with Eq. (13), the expression for $\delta\phi$ can be written as

$$\delta\phi = S_\alpha \delta u'_\alpha \quad \text{with} \quad S_1 = -\frac{u'_2}{D}, \quad S_2 = \frac{1+u'_1}{D} \quad \text{and} \quad D = (1+u'_1)^2 + u'^2_2. \tag{26}$$

From the expression for the first Piola–Kirchhoff stress $\mathbf{P}$ in Eq. $(25)_1$ and using $(21)_{1,2}$ it follows that the Cauchy stress $\boldsymbol{\sigma}$ takes the form

$$\boldsymbol{\sigma} = \left(J^{-1}\mathbf{P}\mathbf{F}^{\top}\right)_{J=1} = \mu(\boldsymbol{\Lambda} + \alpha\boldsymbol{\Psi}) - P^*\mathbf{I}, \tag{27}$$

which is an asymmetric tensor in LCEs, in general. Now, employing the plane stress assumption $\sigma_{33} = 0$ to determine the Lagrange multiplier P^*, we obtain:

$$P^* = \mu\Lambda_{33} = \mu R_0^{-1} R\lambda^2 = \mu R_0^{-1} R\hat{J}^{-2}, \tag{28}$$

where use has been made of Eqs. $(5)_1$, $(7)_1$, and (9) alongside $\Psi_{33} = 0$.

In the subsequent step, to derive the expression for the element stiffness matrix in the nonlinear finite element formulation, it is needed to compute the increment of the virtual internal energy $\Delta\delta\mathcal{U}$. Accordingly, from Eq. (24) one may write

$$\begin{aligned} \Delta\delta\mathcal{U} =& \delta\mathbf{F} : \left(\boldsymbol{\mathcal{A}}^{(1)} : \Delta\mathbf{F} + \boldsymbol{\mathcal{A}}^{(2)} : \Delta\hat{\mathbf{F}} + \mathbf{D}^{(1)}\Delta\theta\right) + \delta\theta\left(\mathbf{D}^{(1)} : \Delta\mathbf{F} + H^{(1)}\Delta\theta\right) \\ &+ \delta\phi\left(\mathbf{D}^{(2)} : \Delta\mathbf{F} + H^{(2)}\Delta\theta + H^{(3)}\Delta\phi\right) + \mathbf{P} : \Delta\delta\mathbf{F} + T\Delta\delta\phi, \end{aligned} \tag{29}$$

where the fourth-order tensors $\boldsymbol{\mathcal{A}}(\mathcal{I})$, the second-order tensors $\mathbf{D}^{(\mathcal{I})}$ $(\mathcal{I} = 1, 2)$, and the scalar functions $H^{(\mathcal{J})}$ $(\mathcal{J} = 1, 2, 3)$ are defined as follows:

$$\left.\begin{aligned}
\boldsymbol{\mathcal{A}}^{(1)} = \mu\big(\tilde{\mathbf{L}} \boxtimes \mathbf{L}_0 + \alpha \mathbf{N} \boxtimes \bar{\mathbf{N}}_0\big) + P^* \mathbf{F}^{-\top} \odot \mathbf{F}^{-\top}, \quad \boldsymbol{\mathcal{A}}^{(2)} = 2P^* \mathbf{F}^{-\top} \otimes \hat{\mathbf{F}}^{-\top} \\
\mathbf{D}^{(1)} = \mathbf{P}_{,\theta} = Q_{,\mathbf{F}} = \mu\big(\tilde{\mathbf{L}}_{,\theta} \mathbf{F} \mathbf{L}_0 + \alpha \mathbf{N}_{,\theta} \mathbf{F} \bar{\mathbf{N}}_0\big), \quad \mathbf{D}^{(2)} = T_{,\mathbf{F}} = \mu \tilde{\mathbf{L}}_{,\phi} \mathbf{F} \mathbf{L}_0 \\
H^{(1)} = Q_{,\theta} = \frac{1}{2}\mu \mathrm{tr}\left(\tilde{\mathbf{L}}_{,\theta\theta} \mathbf{F} \mathbf{L}_0 \mathbf{F}^\top + \alpha \mathbf{N}_{,\theta\theta} \mathbf{F} \bar{\mathbf{N}}_0 \mathbf{F}^\top\right) \\
H^{(2)} = T_{,\theta} = \frac{1}{2}\mu \mathrm{tr}\left(\tilde{\mathbf{L}}_{,\theta\phi} \mathbf{F} \mathbf{L}_0 \mathbf{F}^\top\right), \quad H^{(3)} = T_{,\phi} = \frac{1}{2}\mu \mathrm{tr}\left(\tilde{\mathbf{L}}_{,\phi\phi} \mathbf{F} \mathbf{L}_0 \mathbf{F}^\top\right)
\end{aligned}\right\}. \tag{30}$$

The tensor $\hat{\mathbf{F}}$ in Eq. $(30)_2$ is identical to the deformation gradient tensor $\mathbf{F}$ given in Eq. (3), except that the thickness stretch λ is replaced with 1. Moreover, the expression for $\Delta\delta\phi$ may be written as follows:

$$\Delta\delta\phi = S_3(\delta u_1' \Delta u_2' + \delta u_2' \Delta u_1') + S_4(\delta u_1' \Delta u_1' - \delta u_2' \Delta u_2'), \tag{31}$$

where the functions S_3 and S_4 are given by

$$S_3 = \frac{u_2'^2 - (1+u_1')^2}{D^2}, \quad S_4 = \frac{2u_2'(1+u_1')}{D^2}. \tag{32}$$

Next, let $\boldsymbol{\mathcal{B}}$ be a generic member of the set $\{\mathbf{F}, F_{\alpha\beta}, \lambda, \hat{J}, \mathbf{P}, Q, \boldsymbol{\mathcal{A}}^{(\mathcal{I})}, \mathbf{D}^{(\mathcal{I})}, H^{(\mathcal{J})}\}$. By neglecting higher-order terms in X_2, one may approximately write $\boldsymbol{\mathcal{B}} = \boldsymbol{\mathcal{B}}^{(0)} + X_2 \boldsymbol{\mathcal{B}}^{(1)}$. In particular, from Eq. $(5)_2$, the expressions for $\hat{\boldsymbol{J}}^{(0)}$ and $\hat{\boldsymbol{J}}^{(1)}$ are calculated to be

$$\left.\begin{aligned}
\hat{\boldsymbol{J}}^{(0)} = \det \mathbf{F}^{(0)} = F_{11}^{(0)} F_{22}^{(0)} - F_{12}^{(0)} F_{21}^{(0)} \\
\hat{\boldsymbol{J}}^{(1)} = \hat{\boldsymbol{J}}^{(0)} \mathrm{tr}(\mathbf{F}^{(0)-1} \mathbf{F}^{(1)}) = F_{11}^{(0)} F_{22}^{(1)} + F_{11}^{(1)} F_{22}^{(0)} - F_{12}^{(0)} F_{21}^{(1)} - F_{12}^{(1)} F_{21}^{(0)}
\end{aligned}\right\}. \tag{33}$$

Moreover, from Eqs $(5)_1$ and (33), one obtains $\lambda^{(0)}$ and $\lambda^{(1)}$ as follows:

$$\lambda^{(0)} = \hat{\boldsymbol{J}}^{(0)-1}, \quad \lambda^{(1)} = -\hat{\boldsymbol{J}}^{(1)} \hat{\boldsymbol{J}}^{(0)-2}. \tag{34}$$

Now, from Eq. (24), the virtual internal energy $\delta\hat{\mathcal{U}}$ takes the form

$$\delta\hat{\mathcal{U}} = \int_{V_0} \delta\mathcal{U} \mathrm{d}V_0 = \int_{X_1=0}^{X_1=L} \left[I_0 \mathbf{P}^{(1)} : \delta\mathbf{F}^{(1)} + A_0\big(\mathbf{P}^{(0)} : \delta\mathbf{F}^{(0)} + Q^{(0)}\delta\theta + T^{(0)}\delta\phi\big)\right] \mathrm{d}X_1, \tag{35}$$

where V_0, A_0, and I_0 represent the reference volume, cross-sectional area, and the moment of inertia about the X_3-axis, respectively. Similarly, based on Eq. (29), the incremental virtual internal energy $\Delta\delta\hat{\mathcal{U}}$ may be written as

$$\begin{aligned}\Delta\delta\hat{\mathcal{U}} = \int_{X_1=0}^{X_1=L} \Big\{ A_0 \Big[&\delta\mathbf{F}^{(0)} : \big(\boldsymbol{\mathcal{A}}^{(10)} : \Delta\mathbf{F}^{(0)} + \boldsymbol{\mathcal{A}}^{(20)} : \Delta\hat{\mathbf{F}}^{(0)} + \mathbf{D}^{(10)}\Delta\theta\big) + \delta\theta\big(\mathbf{D}^{(10)} : \Delta\mathbf{F}^{(0)} + H^{(10)}\Delta\theta\big) \\ &+ \delta\phi\big(\mathbf{D}^{(20)} : \Delta\mathbf{F}^{(0)} + H^{(20)}\Delta\theta + H^{(30)}\Delta\phi\big) + T^{(0)}\Delta\delta\phi \Big] \\ &+ I_0 \Big[\delta\mathbf{F}^{(1)} : \big(\boldsymbol{\mathcal{A}}^{(10)} : \Delta\mathbf{F}^{(1)} + \boldsymbol{\mathcal{A}}^{(11)} : \Delta\mathbf{F}^{(0)} + \boldsymbol{\mathcal{A}}^{(20)} : \Delta\hat{\mathbf{F}}^{(1)} + \boldsymbol{\mathcal{A}}^{(21)} : \Delta\hat{\mathbf{F}}^{(0)}\big) \\ &+ \delta\mathbf{F}^{(0)} : \big(\boldsymbol{\mathcal{A}}^{(11)} : \Delta\mathbf{F}^{(1)} + \boldsymbol{\mathcal{A}}^{(21)} : \Delta\hat{\mathbf{F}}^{(1)}\big) + \delta\mathbf{F}^{(1)} : \mathbf{D}^{(11)}\Delta\theta \\ &+ \big(\delta\theta\mathbf{D}^{(11)} + \delta\phi\mathbf{D}^{(21)}\big) : \Delta\mathbf{F}^{(1)} + \mathbf{P}^{(1)} : \Delta\delta\mathbf{F}^{(1)} \Big] \Big\} \mathrm{d}X_1. \end{aligned} \tag{36}$$

In the following section, Eq. (36) is used to derive the expression for the element stiffness matrix.

4. Finite element formulation using B-spline functions

It has been shown that finite element formulations based on B-splines exhibit superior convergence properties (e.g., Refs. [71, 78, 79]). Accordingly, in this section, we develop the finite element formulation of the current LCE beam problem using B-spline functions.

To define B-spline functions of order p over the real interval $[a, b]$, with $b > a$, a knot vector $\boldsymbol{\Xi}$ is first considered. This vector comprises m non-decreasing real numbers, denoted as $\boldsymbol{\Xi} = \{\xi_1, \xi_2, ..., \xi_m\}$. Here, $\xi_1 = a$, $\xi_m = b$, $m = p + q + 1$ is the number of members in $\boldsymbol{\Xi}$, and q is the number of B-splines. The knot vector is said to be open if a and b have the multiplicity of $p + 1$. In this work, open knot vectors are utilized. For a given knot vector $\boldsymbol{\Xi}$, the univariate B-spline basis functions $N_{\mathcal{I}}^p$ ($\mathcal{I} = 1, 2, ..., q$) and their first-order derivative are defined recursively by the following relations [78]:

$$N_{\mathcal{I}}^p = \frac{\xi - \xi_{\mathcal{I}}}{a_1} N_{\mathcal{I}}^{p-1} + \frac{\xi - \xi_{\mathcal{I}+p+1}}{a_2} N_{\mathcal{I}+1}^{p-1}, \quad N_{\mathcal{I},\xi}^p = p\left(\frac{1}{a_1} N_{\mathcal{I}}^{p-1} + \frac{1}{a_2} N_{\mathcal{I}+1}^{p-1}\right), \tag{37}$$

where $a_1 = \xi_{\mathcal{I}+p} - \xi_{\mathcal{I}}$ and $a_2 = \xi_{\mathcal{I}+1} - \xi_{\mathcal{I}+p+1}$. It is noted that for $p = 1$, B-splines of the form $N_{\mathcal{I}}^0(\xi)$ are required. These functions represent piecewise constant functions $N_{\mathcal{I}}^0$, defined as $N_{\mathcal{I}}^0(\xi) = 1$ if $\xi_{\mathcal{I}} \leq \xi < \xi_{\mathcal{I}+1}$ and $N_{\mathcal{I}}^0(\xi) = 0$ otherwise. Additionally, we adhere to the convention $0/0 = 0$ in B-spline calculations. Further insights into B-spline functions can be explored in the existing literature (e.g., [78, 80]). For simplicity, we drop the superscript p in $N_{\mathcal{I}}^p$. A one-dimensional B-spline curve is characterized by B-spline functions $N_{\mathcal{I}}$ and a set of q predetermined control points

$\mathbb{Z}_{\mathcal{I}}$ as follows:

$$\mathbb{x}(\xi) = \sum_{\mathcal{I}=1}^{q} N_{\mathcal{I}}(\xi)\mathbb{Z}_{\mathcal{I}}. \tag{38}$$

In one dimensional finite element method using B-splines, the interval $[\xi_{\mathcal{I}}, \xi_{\mathcal{I}+1}]$ between two distinct knots defines an element $\hat{\Omega}$ in the parametric space. This parametric element can be mapped to the corresponding physical element Ω using Eq. (38).

It is recalled that u_1, u_2, w_1, w_2, η, and θ represent the unknown field variables in the current formulation. To simplify and compactly represent all variables, we use the notation $v_{\mathcal{I}}$ ($\mathcal{I} = 1, 2, ..., 6$), so that

$$v_1 = u_1, \quad v_2 = u_2, \quad v_3 = w_1, \quad v_4 = w_2, \quad v_5 = \eta, \quad v_6 = \theta. \tag{39}$$

Each field variable $v_{\mathcal{I}}$ is approximated via a set of distinct B-spline functions $N_{\mathcal{I}\mathcal{J}}$ of order $p_{\mathcal{I}}$ in the following form:

$$v_{\mathcal{I}}(X_1) = \sum_{\mathcal{J}=1}^{q_{\mathcal{I}}} N_{\mathcal{I}\mathcal{J}}(X_1)V_{\mathcal{I}\mathcal{J}}, \qquad \mathcal{I} = 1, 2, ..., 6, \tag{40}$$

where $V_{\mathcal{I}\mathcal{J}}$ represents the field $v_{\mathcal{I}}$ at the $\mathcal{J}^{\text{th}}$ control point, and $q_{\mathcal{I}}$ is the number of B-splines corresponding to $v_{\mathcal{I}}$. To introduce a shorthand notation, the column vectors $\mathbb{V}_{\mathcal{I}}$, and the row vectors $\mathbb{N}_{\mathcal{I}}$ and $\mathbb{B}_{\mathcal{I}}$ ($\mathcal{I} = 1, 2, ..., 6$) are defined as

$$\mathbb{V}_{\mathcal{I}} = \{V_{\mathcal{I}1}, V_{\mathcal{I}2}, ..., V_{\mathcal{I}q_{\mathcal{I}}}\}^{\mathsf{T}}, \quad \mathbb{N}_{\mathcal{I}} = \{N_{\mathcal{I}1}, N_{\mathcal{I}2}, ..., N_{\mathcal{I}q_{\mathcal{I}}}\}, \quad \mathbb{B}_{\mathcal{I}} = \{N'_{\mathcal{I}1}, N'_{\mathcal{I}2}, ..., N'_{\mathcal{I}q_{\mathcal{I}}}\}. \tag{41}$$

From Eqs. (40) and (41) it follows that each field variable $v_{\mathcal{I}}$ and its derivative $v'_{\mathcal{I}}$ may be written as

$$v_{\mathcal{I}}(X_1) = \mathbb{N}_{\mathcal{I}}(X_1)\mathbb{V}_{\mathcal{I}}, \quad v'_{\mathcal{I}}(X_1) = \mathbb{B}_{\mathcal{I}}(X_1)\mathbb{V}_{\mathcal{I}}, \quad \mathcal{I} = 1, 2, ..., 6, \quad \text{(no sum on I)}. \tag{42}$$

The generalized displacement vector $\mathbb{V}$ over a typical element is then defined as follows:

$$\mathbb{V}_{\tilde{n}\times 1} = \{\mathbb{V}_1^{\mathsf{T}}, \mathbb{V}_2^{\mathsf{T}}, ..., \mathbb{V}_6^{\mathsf{T}}\}^{\mathsf{T}} \quad \text{with} \quad \tilde{n} = \sum_{\mathcal{I}=1}^{6} q_{\mathcal{I}}. \tag{43}$$

Based on Eqs. (4), and (41)–(43), variations of $F^{(\mathcal{I})}_{\alpha\beta}$ ($\mathcal{I} = 0, 1$), u'_α, w_α, ψ, and θ in terms of the virtual generalized displacement vector $\delta\mathbb{V}$ can be expressed as

$$\{\delta F^{(\mathcal{I})}_{\alpha\beta}, \delta u_\alpha, \delta u'_\alpha, \delta w_\alpha, \delta\psi, \delta\theta\} = \{\mathbb{B}_{\mathcal{I}\alpha\beta}, \mathbb{N}_{u\alpha}, \mathbb{B}_{u\alpha}, \mathbb{N}_{w\alpha}, \mathbb{N}_\psi, \mathbb{N}_\theta\}\delta\mathbb{V}, \tag{44}$$

where the row vectors $\mathbb{B}_{\mathcal{I}\alpha\beta}$, $\mathbb{B}_{u\alpha}$, $\mathbb{N}_{w\alpha}$, $\mathbb{N}_\psi$, and $\mathbb{N}_\theta$ are given by

$$\left.\begin{aligned}
\mathbb{B}_{011} = [\mathbb{B}_1, \mathbb{0}, \mathbb{0}, \mathbb{0}, \mathbb{0}, \mathbb{0}], \quad \mathbb{B}_{012} = [\mathbb{0}, \mathbb{0}, \mathbb{N}_3, \mathbb{0}, \mathbb{0}, \mathbb{0}], \quad \mathbb{B}_{021} = [\mathbb{0}, \mathbb{B}_2, \mathbb{0}, \mathbb{0}, \mathbb{0}, \mathbb{0}] \\
\mathbb{B}_{022} = [\mathbb{0}, \mathbb{0}, \mathbb{0}, \upsilon_5\mathbb{N}_4, \mathbb{0}, \mathbb{0}], \quad \mathbb{B}_{111} = [\mathbb{0}, \mathbb{0}, \mathbb{B}_3, \mathbb{0}, \mathbb{0}, \mathbb{0}], \quad \mathbb{B}_{112} = 2[\mathbb{0}, \mathbb{0}, \upsilon_5\mathbb{N}_3, \mathbb{0}, \upsilon_3\mathbb{N}_5, \mathbb{0}] \\
\mathbb{B}_{121} = 2[\mathbb{0}, \mathbb{0}, \mathbb{0}, \mathbb{B}_4, \mathbb{0}, \mathbb{0}], \quad \mathbb{B}_{122} = 2[\mathbb{0}, \mathbb{0}, \upsilon_5\mathbb{N}_4, \mathbb{0}, (1+\upsilon_4)\mathbb{N}_5, \mathbb{0}] \\
\mathbb{N}_{u1} = [\mathbb{N}_1, \mathbb{0}, \mathbb{0}, \mathbb{0}, \mathbb{0}, \mathbb{0}], \quad \mathbb{N}_{u2} = [\mathbb{0}, \mathbb{N}_2, \mathbb{0}, \mathbb{0}, \mathbb{0}, \mathbb{0}], \quad \mathbb{B}_{u1} = [\mathbb{B}_1, \mathbb{0}, \mathbb{0}, \mathbb{0}, \mathbb{0}, \mathbb{0}] \\
\mathbb{B}_{u2} = [\mathbb{0}, \mathbb{B}_2, \mathbb{0}, \mathbb{0}, \mathbb{0}, \mathbb{0}], \quad \mathbb{N}_{w1} = [\mathbb{0}, \mathbb{0}, \mathbb{N}_3, \mathbb{0}, \mathbb{0}, \mathbb{0}], \quad \mathbb{N}_{w2} = [\mathbb{0}, \mathbb{0}, \mathbb{0}, \mathbb{N}_4, \mathbb{0}, \mathbb{0}] \\
\mathbb{N}_\psi = [\mathbb{0}, \mathbb{0}, \mathbb{0}, \mathbb{0}, \mathbb{N}_5, \mathbb{0}], \quad \mathbb{N}_\theta = [\mathbb{0}, \mathbb{0}, \mathbb{0}, \mathbb{0}, \mathbb{0}, \mathbb{N}_6]
\end{aligned}\right\}. \tag{45}$$

Motivated by Eqs. (33) and (34), partial derivatives of $\delta\lambda^{(0)}$ and $\delta\lambda^{(1)}$ with respect to $F^{(0)}_{\alpha\beta}$ and $F^{(1)}_{\alpha\beta}$ are expressed as

$$W_{\alpha\beta} = \frac{\partial\lambda^{(0)}}{\partial F^{(0)}_{\alpha\beta}} = \frac{\partial\lambda^{(1)}}{\partial F^{(1)}_{\alpha\beta}}, \quad Z_{\alpha\beta} = \frac{\partial\lambda^{(1)}}{\partial F^{(0)}_{\alpha\beta}}, \tag{46}$$

from which the expressions for $\delta\lambda^{(0)}$ and $\delta\lambda^{(1)}$ are obtained as

$$\delta\lambda^{(0)} = W_{\alpha\beta}\delta F^{(0)}_{\alpha\beta}, \quad \delta\lambda^{(1)} = Z_{\alpha\beta}\delta F^{(0)}_{\alpha\beta} + W_{\alpha\beta}\delta F^{(1)}_{\alpha\beta}. \tag{47}$$

From Eqs. $(44)_1$ and (47), the vectorial representation of $\delta\mathbf{F}_I$ ($I = 0, 1$) may be written in the following form:

$$\left.\begin{aligned}
\delta\mathbb{F}_0 &\overset{\text{def}}{=} \{\delta F^{(0)}_{11}, \delta F^{(0)}_{22}, \delta F^{(0)}_{12}, \delta F^{(0)}_{21}, \delta\lambda^{(0)}\}^\top = \mathbb{B}_{F0}\delta\mathbb{V} \\
\delta\mathbb{F}_1 &\overset{\text{def}}{=} \{\delta F^{(1)}_{11}, \delta F^{(1)}_{22}, \delta F^{(1)}_{12}, \delta F^{(1)}_{21}, \delta\lambda^{(1)}\}^\top = \mathbb{B}_{F1}\delta\mathbb{V}
\end{aligned}\right\}. \tag{48}$$

where $\mathbb{B}_{F0}$ and $\mathbb{B}_{F1}$ are given by

$$\mathbb{B}_{F0} = \begin{bmatrix} \mathbb{B}_{011} \\ \mathbb{B}_{022} \\ \mathbb{B}_{012} \\ \mathbb{B}_{021} \\ W_{\alpha\beta}\mathbb{B}_{0\alpha\beta} \end{bmatrix}, \quad \mathbb{B}_{F1} = \begin{bmatrix} \mathbb{B}_{111} \\ \mathbb{B}_{122} \\ \mathbb{B}_{112} \\ \mathbb{B}_{121} \\ Z_{\alpha\beta}\mathbb{B}_{0\alpha\beta} + W_{\alpha\beta}\mathbb{B}_{1\alpha\beta} \end{bmatrix}. \tag{49}$$

Substituting Eqs. $(44)_{2-4}$ and (44) into (35), the discretized form of the virtual internal energy $\delta\hat{\mathcal{U}}$ is obtained to be

$$\delta\hat{\mathcal{U}} = \delta\mathbb{V}^{\mathsf{T}}\mathbb{F}^{\text{int}} \quad \text{with} \quad \mathbb{F}^{\text{int}} = \int_{\mathcal{L}_{\text{e}}} \left[A_0\big(\mathbb{B}_{F0}^{\mathsf{T}}\mathbb{P}^{(0)} + \boldsymbol{Q}^{(0)}\mathbb{N}_{\theta}^{\mathsf{T}} + \boldsymbol{T}^{(0)}\mathbb{B}_{\phi}^{\mathsf{T}}\big) + I_0\mathbb{B}_{F1}^{\mathsf{T}}\mathbb{P}^{(1)}\right]\mathrm{d}X_1, \tag{50}$$

where $\boldsymbol{\mathcal{L}}_{\text{e}}$ indicates integration over the length of the element, $\mathbb{B}_{\phi} = S_1\mathbb{B}_{u1} + S_2\mathbb{B}_{u2}$, and $\mathbb{F}^{\text{int}}$ is the internal force vector. For the case of light loading, both the virtual external work $\delta\hat{\mathcal{W}}$ and the external force vector $\mathbb{F}^{\text{ext}}$ are identically zero. Additionally, from Eqs. (36), (44), and (49) the stiffness matrix $\mathbb{K}$ of the typical element Ω is given by

$$\begin{aligned} \mathbb{K} = \int_{\mathcal{L}_{\text{e}}} \Big\{ & A_0\big[\mathbb{B}_{F0}^{\mathsf{T}}\big(\mathbb{A}^{(10)}\mathbb{B}_{F0} + \mathbb{A}^{(20)}\mathbb{B}_{\hat{F}0} + \mathbb{D}^{(10)\mathsf{T}}\mathbb{N}_{\theta}\big) + \mathbb{N}_{\theta}^{\mathsf{T}}\big(\mathbb{D}^{(10)}\mathbb{B}_{F0} + \boldsymbol{H}^{(10)}\mathbb{N}_{\theta}\big) \\ & + \mathbb{B}_{\phi}^{\mathsf{T}}\big(\mathbb{D}^{(20)}\mathbb{B}_{F0} + \boldsymbol{H}^{(20)}\mathbb{N}_{\theta} + \boldsymbol{H}^{(30)}\mathbb{B}_{\phi}\big) + \boldsymbol{T}^{(0)}(S_3\mathbb{K}_{\phi}^{(1)} + S_4\mathbb{K}_{\phi}^{(2)})\big] \\ & + I_0\big[\mathbb{B}_{F1}^{\mathsf{T}}\big(\mathbb{A}^{(10)}\mathbb{B}_{F1} + \mathbb{A}^{(20)}\mathbb{B}_{\hat{F}1} + \mathbb{A}^{(11)}\mathbb{B}_{F0} + \mathbb{A}^{(21)}\mathbb{B}_{\hat{F}0} + \mathbb{D}^{(11)}\mathbb{N}_{\theta}\big) \\ & + \mathbb{B}_{F0}^{\mathsf{T}}\big(\mathbb{A}^{(11)}\mathbb{B}_{F1} + \mathbb{A}^{(21)}\mathbb{B}_{\hat{F}1}\big) + \big(\mathbb{N}_{\theta}^{\mathsf{T}}\mathbb{D}^{(11)} + \mathbb{B}_{\phi}^{\mathsf{T}}\mathbb{D}^{(21)}\big)\mathbb{B}_{F1} + \boldsymbol{P}_{12}^{(1)}\mathbb{K}_{12}^{(1)} + \boldsymbol{P}_{22}^{(1)}\mathbb{K}_{22}^{(1)}\big] \Big\}\mathrm{d}X_1, \end{aligned} \tag{51}$$

where the matrices $\mathbb{B}_{\hat{F}\mathcal{I}}$ ($\mathcal{I} = 0, 1$) are the same as $\mathbb{B}_{F\mathcal{I}}$ in Eq. (49) except that their last row is set to zero. Moreover, the sub-matrices $\mathbb{K}_{\phi}^{(1)}$, $\mathbb{K}_{\phi}^{(2)}$, $\mathbb{K}_{12}^{(1)}$ and $\mathbb{K}_{22}^{(1)}$ are as follows:

$$\left.\begin{aligned} \mathbb{K}_{\phi}^{(1)} &= \mathbb{B}_{u1}^{\mathsf{T}}\mathbb{B}_{u2} + \mathbb{B}_{u2}^{\mathsf{T}}\mathbb{B}_{u1}, \quad \mathbb{K}_{\phi}^{(2)} = \mathbb{B}_{u1}^{\mathsf{T}}\mathbb{B}_{u1} - \mathbb{B}_{u2}^{\mathsf{T}}\mathbb{B}_{u2} \\ \mathbb{K}_{12}^{(1)} &= \mathbb{N}_{\psi}^{\mathsf{T}}\mathbb{N}_{w1} + \mathbb{N}_{w1}^{\mathsf{T}}\mathbb{N}_{\psi}, \quad \mathbb{K}_{22}^{(1)} = \mathbb{N}_{\psi}^{\mathsf{T}}\mathbb{N}_{w2} + \mathbb{N}_{w2}^{\mathsf{T}}\mathbb{N}_{\psi} \end{aligned}\right\}. \tag{52}$$

Furthermore, from the motion field given in Eq. (1), the mass matrix of the typical element is approximately given by

$$\mathbb{M} = \int_{\mathcal{L}_{\text{e}}} \rho_0 A_0\big(\mathbb{N}_{u1}^{\mathsf{T}}\mathbb{N}_{u1} + \mathbb{N}_{u2}^{\mathsf{T}}\mathbb{N}_{u2}\big)\mathrm{d}X_1, \tag{53}$$

where ρ_0 is the reference mass density of the beam. It is noted that due to the small thickness leading to a small value for the moment of inertia, contributions from the director difference vector are neglected. Now, having the expression

for $\mathbb{K}$, $\mathbb{M}$, and $\mathbb{F}^{\text{int}}$, any dynamic algorithm can be used for the time-dependent analysis of LCE beams. In this work, the well-known Newmark method is employed, details of whish are available in many textbooks (e.g., Wriggers [81]).

5. Numerical examples

In this section, we evaluate the performance of the developed formulation through three numerical examples. To obtain numerical solutions, a home-written finite element code based on the developed formulation has been prepared. We utilize the standard 2-point Gauss–Legendre integration rule to evaluate the integrals present in the element stiffness matrix and the internal force vector. Through various numerical simulations, the B-spline functions of degrees $q_1 = 3$, $q_2 = q_3 = q_4 = q_6 = 2$, and $q_5 = 1$ sufficiently approximate the unknown field variables v_1 to v_6 in Eq. (39). However, it is worth noting that higher-degree B-spline functions could also be employed, although they are not considered in this work. In all simulations, the non-ideality parameter is set to be $\alpha = 0.05$. Moreover, due to the incomprehensibility of LCEs, the relation between the shear modulus μ and the Young's modulus E is given by $\mu = E/3$.

5.1. Non-uniform bending of a cantilever LCE beam towards light

In this example, we consider a cantilever beam composed of LCEs subjected to light loading above its top surface. This scenario has been experimentally investigated by White et al. [29]. The light source illuminates in the $-\mathbb{e}_2$ direction, indicating that $\phi_0 = 0$ (see Fig. 1). The apparent intensity of the light is $\mathcal{I}_0 = 1000$ mW/cm^2. However, due to deformation, the effective intensity acting on the beam surface will be $\mathcal{I}_0 \cos\phi$, which leads to non-uniform light loading and non-uniform bending. The length, width, and height of the beam are $L = 6$ mm, $b = 1$ mm, and $h = 8$ μm, respectively. The reference director is along the length of the beam, i.e. $\mathbb{n}_0 = \mathbb{e}_1$. The initial value of the anisotropy parameter is assumed to be $r_0 = 1$. The material properties are specified as follows: Young modulus $E = 1$GPa, density $\rho = 1200$ kg/m^3, adsorption constant $\Gamma = 0.001$ m^2/J, light penetration depth $d = 0.5$ μm, *cis* lifetime $\tau = 0.35$ s, and chemical contraction coefficient $C_{\mathfrak{ch}} = 0.021$. Moreover, the time response is calculated for $t_{\max} = 2$ s.

Through multiple numerical simulations, it was determined that 20 elements are required to obtain convergent results. Variation of the tip slope angle ϕ^T, and the tip displacement components $|u_1^T|$ and u_2^T (scaled by 10) of the beam are displayed in Fig. 2(a). The maximum values of the mentioned parameters are obtained to be $\phi^T_{\max} = 73.87°$, $u^T_{1\max} = 2.75$ mm, and $u^T_{2\max} = 4.53$ mm, respectively. Moreover, it is observed that the curve corresponding to the time history of the tip slope angle ϕ^T are in good agreement with the experimental data reported by White et al. [29].

Deformed shapes of the beam at various time values, namely $t \in \{0.1, 0.2, ..., 0.9, 1, 1.2, 1.5, 2\}$ are illustrated in Fig. 2(b). The curves in Fig. 2(a) and (b) lead to the conclusion that for $t \geq 1.5$, the deformation nearly reaches a saturated state. This is evidenced by the close proximity of the curves corresponding to $t = 1.5$ s and $t = 2$ s.

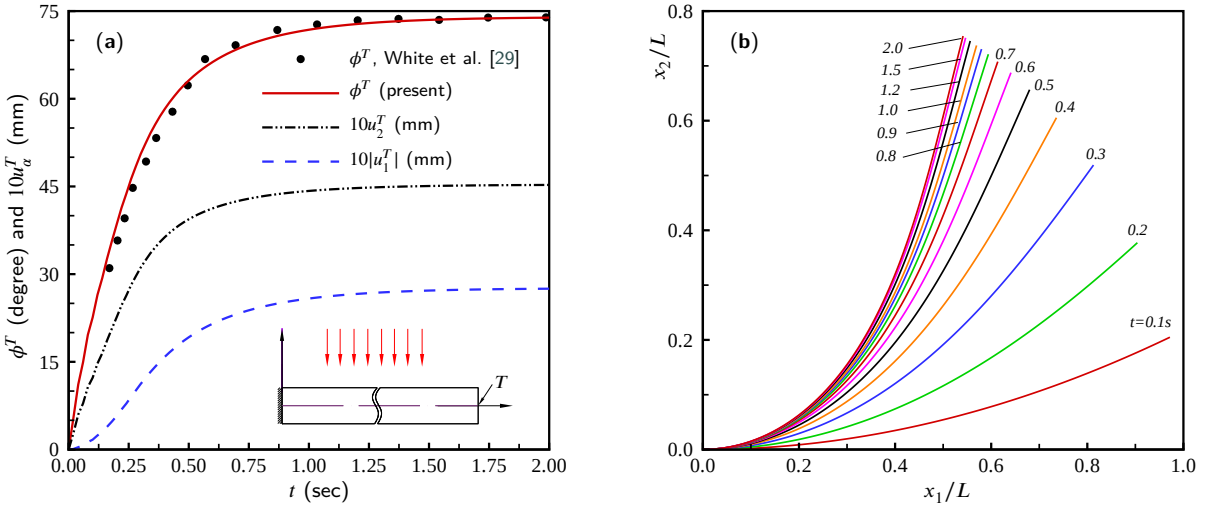

Figure 2: (**a**): Time history of the slope angle ϕ and the displacement components $|u_1|$ and u_2 at the tip point T of the LCE beam, (**b**): deformed shapes of the beam for $t \in \{0.1, 0.2, ..., 0.9, 1, 1.2, 1.5, 2\}$ (s)

5.2. Deformation of an LCE beam under uniform central illumination

In this example, we study the deformation of a beam under a central light source that always acts perpendicular to its top surface. In this scenario, the relative angle $\bar{\phi} = \phi - \phi_0$ in Eq. (14) is identically zero for all points on the beam surface. The problem has been analytically investigated by Corbett and Warner [60] and Goriely et al. [68]. The reference director $\mathbb{n}_0$ is the $\mathbb{e}_1$ direction, and the reference anisotropy parameter is $r_0 = 1$. The values of Young's modulus, density, adsorption constant, light penetration depth, *cis* lifetime, and chemical contraction coefficient are considered to be $E = 1$ GPa, $\rho = 1200$ kg/m^3, $\Gamma = 0.001$ m^2/J, $\tau = 0.35$ s, and $C_{c\mathfrak{h}} = 1$, respectively. By defining the dimensionless light intensity parameter $K_0 = \mathcal{I}_0/\mathcal{I}_c = \tau\Gamma\mathcal{I}_0$, the light intensity $\mathcal{I}_0 = \mathcal{I}_c K_0$ at the top surface of the beam is computed. The time response is calculated for $t \in [0, 2]$ s.

The total length of the beam is taken to be $2L$. Due to symmetry, only one-half of the beam is discretized by the proposed beam element. For the numerical simulations, the half-length and width are set to $L = 0.8$ and $b = 1$, respectively. It is worth noting that the value of the width b is arbitrary and can be replaced by any other value. Through several numerical simulations, it was determined that 20 elements along the half-length L are required to achieve convergent results. The variation of the dimensionless parameter $\beta_2 = \kappa d$, with κ as the beam curvature, versus the dimensionless parameter $\beta_1 = h/d$ for various values of the light intensity parameter K_0 is depicted in Fig. 3(a). The results depicted in the figure demonstrate excellent agreement between the new results and those obtained in Refs. [60, 68]. Figure 3(b) illustrates the deformed shapes of the entire beam at different values of time, namely $t \in \{0.05, 0.1, 0.15, 0.2, 0.3, 0.4, 0.5, 0.7, 1\}$ s. The curves in Fig. 3(a) and (b) indicate that a nearly saturated state of deformation is achieved for $t \geq 1.5$. In other words, the deformed shapes remain almost identical for $t \geq 1.5$.

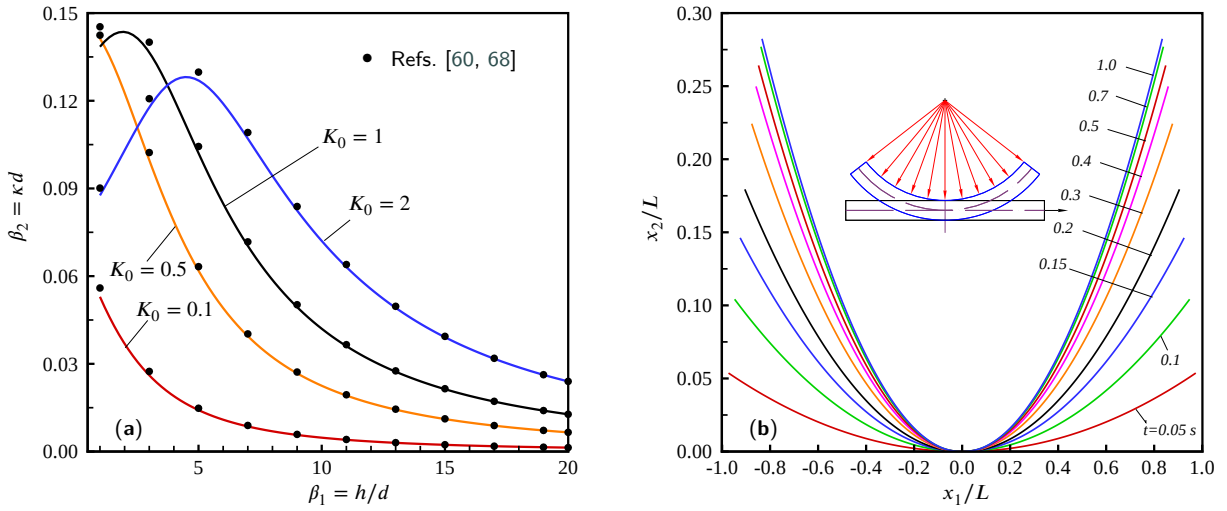

Figure 3: (**a**): Time history of the slope angle ϕ and the displacement components $|u_1|$ and u_2 at the tip point T of the LCE beam, (**b**): deformed shapes of the beam at different times

5.3. Snap-through instability of a clamped-clamped LCE beam

In this example, the snap-through response of an initially buckled LCE beam with clamped-clamped (C-C) boundary conditions under illumination is investigated. This problem has been experimentally studied by Shankar et al. [30]. The beam dimensions are $L = 14.3$ mm in length, $b = 1$ mm in width, and $h = 15$ μm in thickness. The beam is composed of a monodomain liquid crystal network with the reference director $\mathtt{n}_0$ aligned along the X_1-axis, and the reference anisotropy parameter is assumed to be $r_0 = 1$. The Young's modulus, density, *cis* lifetime, and light penetration depth are considered to be $E = 1.25$ GPa, $\rho = 1200$ kg/m^3, $\tau = 0.94$ s, and $d = 8$ μm, respectively. Furthermore, the parameter β in Ref. [30] corresponds to $\tau\Gamma C_{\mathfrak{cfb}}$ in the present formulation and is considered to be 4.8×10^{-5} m^2/W.

The end of the beam at $X_1 = 0$ remains fixed at all times. In the first stage, for the time $t \in [0, 0.2]$ s, the tip of the beam at $X_1 = L$ is subjected to a purely mechanical axial compression, achieving the maximum axial displacement $|u^T_{1\max}| = 0.01L$ at the beam tip. In this position, the maximum lateral deflection $u^M_2/h = 61.98$ (≈ 1 mm) is observed at the midpoint of the beam. In the next stage, the ends of the beam remain fixed, and the beam is subjected to light with an intensity of $\mathcal{I}_0 = 690$ W/m^2. It is noted that only 5 mm of the middle section of the beam is subjected to light loading for $t \in [0.2, 1]$ s.

Numerical simulations reveal that 20 elements are needed to achieve convergent results. Figure 4(a) displays the time history of the displacement components $|u^T_1|$ at the tip and u^M_2 at the midpoint of the beam. After completing the snap-through process, due to inertia effects, minot oscillations in the lateral deflection is observed. This is because damping effects have not been included in the present formulation. Moreover, the data corresponding to the onset of

Table 1
The onset of snap-through $t^{\star}_{\text{s}}$ and the time difference Δt_{s} required to complete it in the C-C beam

$t^{\star}_{\text{s}}$		Δt_{s}	
present	Ref. [30]	present	Ref. [30]
0.7 s	0.7 s	0.08 s	$\approx$ 0.10 s

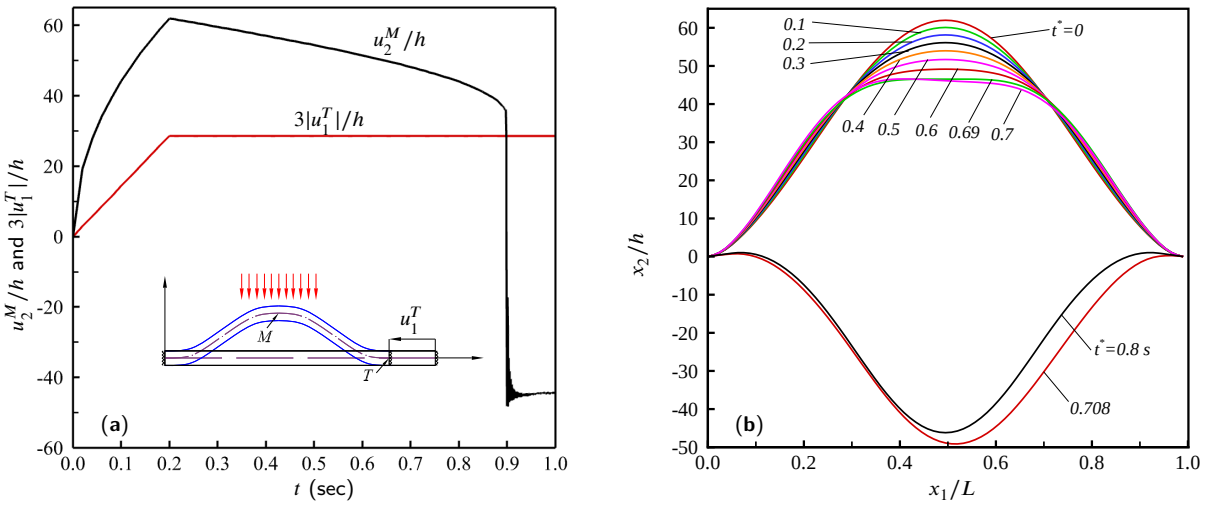

Figure 4: (**a**): The dimensionless displacement components $3|u_1|/h$ at the tip T and u_2/h at the midpoint M of the beam, (**b**): deformed shapes of the beam for $t^{\star} \in \{0, 0.1, ..., 0.6, 0.69, 0.7, 0.708, 0.8\}$ s. Snap-through occurs within the time interval $t^{\star} \in [0.7, 0.708]$ s.

snap-through and its duration are presented in Table 1. It is recalled that the first 0.2 s of time is spent for the purely mechanical compression of the beam. By defining $t^{\star} = t - 0.2$, it is found that the snap through phenomenon starts at $t^{\star} = 0.7$ s, which is coincident with that observed by Shankar et al. [30]. Moreover, in that reference, the time needed to complete the snap-through is approximated to be around 0.10 s. In this work, the calculated time is 0.08 s. In other words, the beam transitions from positive to negative lateral deflection in approximately 0.08 s. The findings in Table 1 demonstrate a high level of concordance between the newly acquired data and the experimental results documented in Shankar et al. [30].

The deformed shapes of the beam at different times, namely $t^{\star} \in \{0, 0.1, ..., 0.6, 0.69, 0.7, 0.708, 0.8\}$ s are illustrated in Figure 4(b). A slight asymmetry in the beam's response is observed at $t^{\star} = 0.708$ s. However, as time progresses to $t^{\star} = 0.8$ s, the final deformed shape becomes symmetrical.

6. Summary

In this paper, a beam formulation for the finite elastic deformation analysis of beam-like structures made of LCEs and stimulated by light was developed. The formulation is applicable to ideal, non-ideal, isotropic genesis, and nematic

genesis LCEs. Notably, the incompressibility constraint is exactly satisfied in the present LCE beam model. The variational form of the problem, based on the principle of virtual work, was formulated. Additionally, a nonlinear finite element formulation based on B-spline functions was presented to solve numerical examples. The applicability of the proposed formulation was examined through three examples. It was demonstrated that the new formulation successfully captures both the experimental and theoretical results already reported in the literature. The modeling framework developed in the present contribution can be applied to the optimal design of sensors and actuators composed of LCEs. Furthermore, it has the potential to incorporate interdisciplinary concepts from fields such as chemistry and mechanical engineering, fostering a synthesis of diverse perspectives in future research.

Declaration of competing interest

The authors declare that they have no known competing financial interests or personal relationships that could have influenced the work reported in this paper.

References

[1] M. Warner, E. M. Terentjev, Liquid Crystal Elastomers, Oxford University Press, 2007.

[2] Y. Zhang, C. Xuan, Y. Jiang, Y. Huo, Continuum mechanical modeling of liquid crystal elastomers as dissipative ordered solids, Journal of the Mechanics and Physics of Solids 126 (2019) 285–303.

[3] W. Gu, X. Qing, J. Wei, Y. Yu, Photoinduced deformation of crosslinked liquid crystalline polymers and soft actuators, Chin. Sci. Bull. 61 (2016) 2102–14.

[4] W. Zhang, Y. Nan, Z. Wu, Y. Shen, D. Luo, Photothermal-driven liquid crystal elastomers: materials, alignment and applications, Molecules 27 (2022) 4330.

[5] A. Varanytsia, H. Nagai, K. Urayama, P. Palffy-Muhoray, Tunable lasing in cholesteric liquid crystal elastomers with accurate measurements of strain, Scientific reports 5 (2015) 17739.

[6] H. Zeng, O. M. Wani, P. Wasylczyk, R. Kaczmarek, A. Priimagi, Self-regulating iris based on light-actuated liquid crystal elastomer, Advanced materials 29 (2017) 1701814.

[7] D. Mistry, N. A. Traugutt, K. Yu, C. M. Yakacki, Processing and reprocessing liquid crystal elastomer actuators, Journal of Applied Physics 129 (2021).

[8] L. Liu, M.-H. Liu, L.-L. Deng, B.-P. Lin, H. Yang, Near-infrared chromophore functionalized soft actuator with ultrafast photoresponsive speed and superior mechanical property, Journal of the American Chemical Society 139 (2017) 11333–6.

[9] Z. Liu, J. Liao, L. He, Q. Gui, Y. Yuan, H. Zhang, Preparation, photo-induced deformation behavior and application of hydrogen-bonded crosslinked liquid crystalline elastomers based on α-cyanostilbene, Polymer Chemistry 11 (2020) 6047–55.

[10] J. Küpfer, H. Finkelmann, Nematic liquid single crystal elastomers, Die Makromolekulare Chemie, Rapid Communications 12 (1991) 717–26.

[11] J. Küpfer, H. Finkelmann, Liquid crystal elastomers: Influence of the orientational distribution of the crosslinks on the phase behaviour and reorientation processes, Macromolecular Chemistry and Physics 195 (1994) 1353–67.

[12] I. Kundler, H. Finkelmann, Strain-induced director reorientation in nematic liquid single crystal elastomers, Macromolecular Rapid Communications 16 (1995) 679–86.

[13] H. Finkelmann, I. Kundler, E. Terentjev, M. Warner, Critical stripe-domain instability of nematic elastomers, Journal de Physique II 7 (1997) 1059–69.

[14] H. Finkelmann, A. Greve, M. Warner, The elastic anisotropy of nematic elastomers, The European Physical Journal E 5 (2001) 281–93.

[15] H. Finkelmann, E. Nishikawa, G. Pereira, M. Warner, A new opto-mechanical effect in solids, Physical Review Letters 87 (2001) 015501.

[16] M. Warner, P. Bladon, E. Terentjev, "Soft elasticity" – deformation without resistance in liquid crystal elastomers, Journal de Physique II 4 (1994) 93–102.

[17] S. Conti, A. DeSimone, G. Dolzmann, Soft elastic response of stretched sheets of nematic elastomers: a numerical study, Journal of the Mechanics and Physics of Solids 50 (2002) 1431–51.

[18] X. He, Y. Zheng, Q. He, S. Cai, Uniaxial tension of a nematic elastomer with inclined mesogens, Extreme Mechanics Letters 40 (2020) 100936.

[19] M. Groß, J. Dietzsch, F. Concas, A new mixed finite element formulation for reorientation in liquid crystalline elastomers, European Journal of Mechanics-A/Solids 97 (2023) 104828.

[20] L. A. Mihai, H. Wang, J. Guilleminot, A. Goriely, Nematic liquid crystalline elastomers are aeolotropic materials, Proceedings of the Royal Society A 477 (2021) 20210259.

[21] L. A. Mihai, D. Mistry, T. Raistrick, H. F. Gleeson, A. Goriely, A mathematical model for the auxetic response of liquid crystal elastomers, Philosophical Transactions of the Royal Society A 380 (2022) 20210326.

[22] L. A. Mihai, A. Goriely, A pseudo-anelastic model for stress softening in liquid crystal elastomers, Proceedings of the Royal Society A 476 (2020) 20200558.

[23] L. A. Mihai, A theoretical liquid crystal elastomer model that mimics the elasticity of cat skin, Mechanics of Soft Materials 5 (2023) 1–7.

[24] C. Ahn, X. Liang, S. Cai, Inhomogeneous stretch induced patterning of molecular orientation in liquid crystal elastomers, Extreme Mechanics Letters 5 (2015) 30–6.

[25] F. Xu, S. Zhao, Thermal wrinkling of liquid crystal polymer shell/core spheres, Extreme Mechanics Letters 40 (2020) 100860.

[26] Z. Wei, R. Bai, Temperature-modulated photomechanical actuation of photoactive liquid crystal elastomers, Extreme Mechanics Letters 51 (2022) 101614.

[27] Q. Guo, Y. Zheng, S. Cai, Modeling and numerical simulation of liquid crystal elastomers with thermo-electro-mechanical coupling, International Journal of Plasticity 171 (2023) 103799.

[28] Y. Yu, M. Nakano, T. Ikeda, Directed bending of a polymer film by light, Nature 425 (2003) 145–.

[29] T. J. White, S. V. Serak, N. V. Tabiryan, R. A. Vaia, T. J. Bunning, Polarization-controlled, photodriven bending in monodomain liquid crystal elastomer cantilevers, Journal of Materials Chemistry 19 (2009) 1080–5.

[30] M. R. Shankar, M. L. Smith, V. P. Tondiglia, K. M. Lee, M. E. McConney, D. H. Wang, L.-S. Tan, T. J. White, Contactless, photoinitiated snap-through in azobenzene-functionalized polymers, Proceedings of the National Academy of Sciences 110 (2013) 18792–7.

[31] A. H. Gelebart, D. Jan Mulder, M. Varga, A. Konya, G. Vantomme, E. Meijer, R. L. Selinger, D. J. Broer, Making waves in a photoactive polymer film, Nature 546 (2017) 632–6.

[32] A. S. Kuenstler, R. C. Hayward, Light-induced shape morphing of thin films, Current Opinion in Colloid & Interface Science 40 (2019) 70–86.

[33] R. Bai, K. Bhattacharya, Photomechanical coupling in photoactive nematic elastomers, Journal of the Mechanics and Physics of Solids 144 (2020) 104115.

[34] H. Chung, J. Choi, J.-H. Yun, M. Cho, Light and thermal responses of liquid-crystal-network films: a finite element study, Physical Review E 91 (2015) 042503.

[35] L. Liu, M. del Pozo, F. Mohseninejad, M. G. Debije, D. J. Broer, A. P. Schenning, Light tracking and light guiding fiber arrays by adjusting the location of photoresponsive azobenzene in liquid crystal networks, Advanced Optical Materials 8 (2020) 2000732.

[36] D. R. Anderson, D. E. Carlson, E. Fried, A continuum-mechanical theory for nematic elastomers, Journal of Elasticity 56 (1999) 33–58.

[37] D. E. Carlson, E. Fried, S. Sellers, Force-free states, relative strain, and soft elasticity in nematic elastomers, Journal of Elasticity 69 (2002) 161–80.

[38] E. Fried, S. Sellers, Orientational order and finite strain in nematic elastomers, The Journal of Chemical Physics 123 (2005).

[39] Y.-C. Chen, E. Fried, Uniaxial nematic elastomers: constitutive framework and a simple application, Proceedings of the Royal Society A: Mathematical, Physical and Engineering Sciences 462 (2006) 1295–314.

[40] E. Fried, S. Sellers, Free-energy density functions for nematic elastomers, Journal of the Mechanics and Physics of Solids 52 (2004) 1671–89.

[41] R. Brighenti, C. G. McMahan, M. P. Cosma, A. Kotikian, J. A. Lewis, C. Daraio, A micromechanical-based model of stimulus responsive liquid crystal elastomers, International Journal of Solids and Structures 219 (2021) 92–105.

[42] R. Brighenti, M. P. Cosma, Multiphysics modelling of light-actuated liquid crystal elastomers, Proceedings of the Royal Society A 479 (2023) 20220417.

[43] V. Agostiniani, A. DeSimone, Ogden-type energies for nematic elastomers, International Journal of Non-Linear Mechanics 47 (2012) 402–12.

[44] S. Conti, A. DeSimone, G. Dolzmann, Semisoft elasticity and director reorientation in stretched sheets of nematic elastomers, Physical Review E 66 (2002) 061710.

[45] A. DeSimone, G. Dolzmann, Macroscopic response of nematic elastomers via relaxation of a class of so(3)-invariant energies, Archive for Rational Mechanics and Analysis 161 (2002) 181–204.

[46] P. Bladon, E. Terentjev, M. Warner, Transitions and instabilities in liquid crystal elastomers, Physical Review E 47 (1993) R3838.

[47] C. D. Modes, K. Bhattacharya, M. Warner, Gaussian curvature from flat elastica sheets, Proceedings of the Royal Society A: Mathematical, Physical and Engineering Sciences 467 (2011) 1121–40.

[48] F. Cirak, Q. Long, K. Bhattacharya, M. Warner, Computational analysis of liquid crystalline elastomer membranes: Changing gaussian curvature without stretch energy, International Journal of Solids and Structures 51 (2014) 144–53.

[49] P. Cesana, P. Plucinsky, K. Bhattacharya, Effective behavior of nematic elastomer membranes, Archive for Rational Mechanics and Analysis 218 (2015) 863–905.

[50] P. Plucinsky, K. Bhattacharya, Microstructure-enabled control of wrinkling in nematic elastomer sheets, Journal of the Mechanics and Physics of Solids 102 (2017) 125–50.

[51] P. Plucinsky, M. Lemm, K. Bhattacharya, Actuation of thin nematic elastomer sheets with controlled heterogeneity, Archive for Rational Mechanics and Analysis 227 (2018) 149–214.

[52] B. A. Kowalski, C. Mostajeran, N. P. Godman, M. Warner, T. J. White, Curvature by design and on demand in liquid crystal elastomers, Physical Review E 97 (2018) 012504.

[53] V. Lee, K. Bhattacharya, Actuation of cylindrical nematic elastomer balloons, Journal of Applied Physics 129 (2021) 114701.

[54] K. Li, Q. Wang, P. Xu, Inflation-induced torsion and bulging of a nematic elastomer balloon, Thin-Walled Structures 170 (2022) 108621.

[55] V. Agostiniani, A. DeSimone, Rigorous derivation of active plate models for thin sheets of nematic elastomers, Mathematics and Mechanics of Solids 25 (2020) 1804–30.

[56] Y. Liu, W. Ma, H.-H. Dai, On a consistent finite-strain plate model of nematic liquid crystal elastomers, Journal of the Mechanics and Physics of Solids 145 (2020) 104169.

[57] L. A. Mihai, A. Goriely, A plate theory for nematic liquid crystalline solids, Journal of the Mechanics and Physics of Solids 144 (2020) 104101.

[58] D. Zhao, Y. Liu, Light-induced spontaneous bending of a simply supported liquid crystal elastomer rectangular plate, Physical Review E 101 (2020) 042701.

[59] W. Qiu, Y. Xu, F. Xu, Y. Huo, Programmable electric-field-induced bending shapes of dielectric liquid crystal elastomer sheets, Extreme Mechanics Letters 60 (2023) 101982.

[60] D. Corbett, M. Warner, Linear and nonlinear photoinduced deformations of cantilevers, Physical review letters 99 (2007) 174302.

[61] C. L. Van Oosten, D. Corbett, D. Davies, M. Warner, C. W. Bastiaansen, D. J. Broer, Bending dynamics and directionality reversal in liquid crystal network photoactuators, Macromolecules 41 (2008) 8592–6.

[62] Q. Luo, L. Tong, Constitutive modeling of photostrictive materials and design optimization of microcantilevers, Journal of Intelligent Material Systems and Structures 20 (2009) 1425–38.

[63] L. Jin, Y. Lin, Y. Huo, A large deflection light-induced bending model for liquid crystal elastomers under uniform or non-uniform illumination, International journal of solids and structures 48 (2011) 3232–42.

[64] Y. Lin, L. Jin, Y. Huo, Quasi-soft opto-mechanical behavior of photochromic liquid crystal elastomer: Linearized stress–strain relations and finite element simulations, International Journal of Solids and Structures 49 (2012) 2668–80.

[65] D. Zhao, Y. Liu, Effect of dynamic soft elasticity on vibration of embedded nematic elastomer timoshenko beams, International Journal of Applied Mechanics 10 (2018) 1850058.

[66] A. M. Parrany, Nonlinear light-induced vibration behavior of liquid crystal elastomer beam, International Journal of Mechanical Sciences 136 (2018) 179–87.

[67] K. Korner, A. S. Kuenstler, R. C. Hayward, B. Audoly, K. Bhattacharya, A nonlinear beam model of photomotile structures, Proceedings of the National Academy of Sciences 117 (2020) 9762–70.

[68] A. Goriely, D. E. Moulton, L. A. Mihai, A rod theory for liquid crystalline elastomers, Journal of Elasticity 153 (2023) 509–32.

[69] R. Norouzikudiani, A. Lucantonio, A. DeSimone, Equilibrium and transient response of photo-actuated liquid crystal elastomer beams, Mechanics Research Communications 131 (2023) 104126.

[70] C. Sansour, Large strain deformations of elastic shells constitutive modelling and finite element analysis, Computer Methods in Applied Mechanics and Engineering 161 (1998) 1–18.

[71] F. Dadgar-Rad, A two-dimensional electro-beam model for large deformation analysis of dielectric polymer actuators, International Journal of Solids and Structures 165 (2019) 104–14.

[72] H. Tokumoto, H. Zhou, A. Takebe, K. Kamitani, K. Kojio, A. Takahara, K. Bhattacharya, K. Urayama, Probing the in-plane liquid-like behavior of liquid crystal elastomers, Science Advances 7 (2021) eabe9495.

[73] D. Corbett, C. Xuan, M. Warner, Deep optical penetration dynamics in photobending, Physical Review E 92 (2015) 013206.

[74] S. Liu, K. Huang, K. Wang, B. Wang, Programmable deformation of liquid crystal elastomer plates subjected to concentrated light illumination, Mechanics of Materials 175 (2022) 104501.

[75] J. Biggins, M. Warner, K. Bhattacharya, Supersoft elasticity in polydomain nematic elastomers, Physical review letters 103 (2009) 037802.

[76] G. Verwey, M. Warner, Compositional fluctuations and semisoftness in nematic elastomers, Macromolecules 30 (1997) 4189–95.

[77] F. C. Frank, On the theory of liquid crystals, Discussions of the Faraday Society 25 (1958) 19–28.

[78] J. A. Cottrell, T. J. R. Hughes, Y. Bazilevs, Isogeometric Analysis: Toward Integration of CAD and FEA, Wiley, 2009.

[79] J. Kiendl, M.-C. Hsu, M. C. Wu, A. Reali, Isogeometric Kirchhoff–Love shell formulations for general hyperelastic materials, Computer Methods in Applied Mechanics and Engineering 291 (2015) 280–303.

[80] C. G. Provatidis, Precursors of Isogeometric Analysis, Springer, 2019.

[81] P. Wriggers, Nonlinear Finite Element Methods, Springer, 2008.